Supporting Information

Pulvers et al. 10.1073/pnas.1010494107

SI Results and Discussion

Generation of *Aspm* Mutant Mice. Two *Aspm* mutant mouse lines were generated from gene trap ES cells obtained from the Sanger Institute Gene Trap Resource. PCR and sequencing of genomic DNA revealed the insertion site of the gene trap vector to be between exons 25 and 26 for the ES cell line AJ0069, and between exons 7 and 8 for the AA0137 cell line (Fig. S1*A*). The mutant mice generated from AJ0069 and AA0137 will be referred to as $Aspm^{exon1\text{-}25}$ and $Aspm^{exon1\text{-}7}$ (1-25 and 1-7 in figures), respectively.

To demonstrate that the endogenous *Aspm* mRNA is lost in the two homozygous mutants, RT-PCR was performed on embryonic day (E) 13.5 whole-embryo RNA (Fig. S1*B*). In WT, only the endogenous WT transcript was present (Fig. S1*B*, *Left* and *Middle*, arrows), and in the heterozygotes, both WT and gene-trapped transcripts were present. However, in homozygotes, only the gene-trapped transcript was present (Fig. S1*B*, *Left* and *Middle*, arrowheads), providing evidence that the endogenous *Aspm* transcript was lost. To demonstrate that the Aspm protein is tagged with β-geo, we performed immunostaining for β-galactosidase (β-gal) together with Aspm, using an antibody against the exon 3–encoded sequence (1), on E10.5 dorsal telencephalon sections (Fig. S1*C*). In $Aspm^{exon1\text{-}7}$ heterozygotes and homozygotes, β-gal and Aspm colocalized at metaphase spindle poles (Fig. S1*C*, arrowheads), whereas β-gal immunoreactivity was lacking in the WT, providing evidence for the tagging of Aspm by β-geo. The same observation was made for $Aspm^{exon1\text{-}25}$ mice.

Generation of Human *ASPM* Transgenic Mice. Transgenic mice expressing the human *ASPM* gene were generated by using a bacterial artificial chromosome (BAC) that contains the human *ASPM* locus. RT-PCR on E13.5 whole-embryo RNA from WT and transgenic mice harboring the human BAC, using mouse *Aspm*-specific and human *ASPM*-specific primers, demonstrated the specific expression of the human transcript (Fig. S1*B*, *Right*). Furthermore, in situ hybridization using mouse *Aspm*-specific and human *ASPM*-specific probes showed that the BAC used directed human *ASPM* expression in the developing brain of transgenic mouse embryos with the same spatial pattern as endogenous mouse Aspm (Fig. S2).

Midbody Localization Defects Caused by Lack of Aspm C-Terminal Region. The subcellular localization of Aspm mutant proteins was investigated by using an antibody against the exon 3–encoded protein sequence (1) for immunostaining on E11.5 dorsal telencephalon sections, together with a centrosome marker, γ-tubulin (Fig. S3*A*), and a midbody marker, Aurora B (Fig. S3*B*). In WT, Aspm was found at spindle poles in metaphase and at the midbody in telophase (1–3). In $Aspm^{exon1\text{-}7}$ homozygotes, the mutant protein localized to metaphase spindle poles, although with weaker immunoreactivity compared with WT (Fig. S3*A*); however, no immunoreactivity was detected at the telophase midbody (Fig. S3*B*). The $Aspm^{exon1\text{-}25}$ mutant protein also localized to metaphase spindle poles (Fig. S3*A*), but the immunoreactivity at the telophase midbody was much reduced (Fig. S3*B*).

***Aspm* Mutant Mice Show No Detectable Effects in Orientation and Modes of Apical Progenitor Cell Division.** The cleavage plane orientation of apically dividing neuroepithelial cells of E11.5 dorsal telencephalon of *Aspm* mutant mice was quantified by measuring chromatid orientation, as revealed by DAPI staining, relative to the ventricular surface, as defined by phospho-vimentin (pVim) staining (Fig. S4*A*). Measurements were made on cells in metaphase (Fig. S4*B*, *Left*) and anaphase or telophase (Fig. S4*B*, *Right*). Results showed that the chromatid orientation of apically dividing cells were unchanged in the two homozygotes compared with WT, indicating that there are no major alterations in cleavage plane orientation in the present Aspm mutants.

To examine the regulation of symmetric vs. asymmetric cell division, in terms of the partitioning of cell constituents, in apically dividing neural progenitor cells, E11.5 dorsal telencephalon sections were immunostained for pan-cadherin to define, by lack of immunostaining, the apical plasma membrane (Fig. S4*C*), and to score in anaphase or telophase whether the predicted cleavage plane would bisect (symmetric) or bypass (asymmetric) the apical domain (1, 4). For this analysis, *Aspm* mutant mice were crossed with *Tis21*-GFP knock-in mice (5), to exclude from the analysis asymmetrically dividing cells (*Tis21*-GFP–positive) already committed to differentiative divisions (4). The actual cleavage plane angles measured in *Tis21*-GFP–negative anaphase or telophase cells of WT and $Aspm^{exon1\text{-}7}$ heterozygotes and homozygotes essentially all fell within 70° and 90° for symmetric divisions and were scattered between 60° and 90° for asymmetric divisions (Fig. S4*D*). Quantification of the proportion of symmetric and asymmetric divisions, expressed as a percentage of the total number of *Tis21*-GFP–negative anaphase or telophase cells analyzed (Fig. S4*E*), revealed no significant change in the ratio of symmetric vs. asymmetric cell divisions of the $Aspm^{exon1\text{-}7}$ homozygote compared with WT.

***Aspm* Mutant Mice Show No Detectable Effects on Neural Progenitor Proliferation and Differentiation During Neurogenesis.** To address whether the microcephaly observed in *Aspm* mutants is due to premature progression of neurogenesis, we quantified the proportion of *Tis21*-GFP–positive neurogenic cells, expressed as a percentage of total cells in the ventricular zone (VZ), delimited by TuJ1 immunostaining, in sections of E11.5 dorsal telencephalon (Fig. S5 *A* and *B*). No significant change was observed in the $Aspm^{exon1\text{-}7}$ homozygote compared with WT.

To address whether, in the mutants, there was a premature generation of basal progenitors (5–7), which would be at the expense of expanding neuroepithelial and radial glial cells, we performed Tbr2 immunostaining (8) and quantified the proportion of Tbr2-positive cells, expressed as a percentage of total cells in the cortical wall, in E13.5 dorsal telencephalon sections (Fig. S5 *C* and *D*, *Upper*). No significant change was observed in the $Aspm^{exon1\text{-}7}$ homozygote compared with WT. Sections were also immunostained for PH3 and TuJ1, to quantify the mitotic index of apical and basal progenitor cells in the VZ plus subventricular zone (SVZ; Fig. S5*D*, *Lower*). No significant change was observed in the $Aspm^{exon1\text{-}7}$ homozygote compared with WT.

To analyze whether neuroepithelial cells arrest in metaphase in *Aspm* mutant mice, E11.5 dorsal telencephalon sections were immunostained for PH3, which is positive from late G2 phase to anaphase (9), and pVim, which is positive throughout mitosis, from prophase to telophase (10), together with DAPI (examples in Fig. S4*A*). First, apical mitoses were categorized into either prometaphase and metaphase, or anaphase and telophase, as determined by DAPI staining, and the proportion out of all apical mitotic figures was calculated (Fig. S5*E*). Results showed that the percentage of the respective phases of mitosis were unchanged in the two homozygotes, indicating no alteration in the duration of these phases. Second, because pVim is positive throughout mitosis, but PH3 is only positive to anaphase, the pVim-positive but

PH3-negative staining reveals the proportion of cells in telophase (Fig. S5*F*). The proportion of PH3-positive and -negative cells expressed as a percentage of all pVim-positive cells was unchanged in the two homozygotes compared with WT. These results indicate that there is no detectable metaphase block or defect in mitotic progression of apically dividing neural progenitor cells in the present *Aspm* mutant mice.

SI Materials and Methods

Mouse Lines and Genotyping. *Aspm* gene trap mutant mouse lines were generated from ES cells [ID: AJ0069, $Aspm^{Gt(AJ0069)Wtsi}$; and AA0137, $Aspm^{Gt(AA0137)Wtsi}$; vector pGT0lxr; obtained from the Sanger Institute Gene Trap Resource] by blastocyst injection, and chimeras with germ line transmission were crossed to C57BL/6JOlaHsd. The exon immediately upstream of the vector insertion site, determined by 5′ RACE, was documented on the gene trap resource database (www.sanger.ac.uk/PostGenomics/genetrap). To determine the precise vector insertion site, PCR on ES cell genomic DNA was performed, using a forward primer targeting the upstream exon and a reverse primer targeting the 5′ end of β-geo, followed by sequencing. Primers used were the following: (exon7-F) 5′-GCCAAAAAGTCCTGAATTGG, (exon25-F) 5′-TTTGTTGTGATCCGAAGCTG, and (β-geo-R) 5′-AGTATCGGCCTCAGGAAGATCG. For the AJ0069 ES cell line, the insertion site was found to be in the intron between exon 25 and 26, 518 nt downstream from the intron start site, followed by vector sequence (starting at nt 288 downstream of the unique HindIII site); for the AA0137 ES cell line, the insertion site was found to be in the intron between exon 7 and 8, 1,386 nt downstream from the intron start site, followed by vector sequence (starting at nt 1,330 downstream of the HindIII site).

On the basis of the insert location, PCR primers for genotyping were designed. For AA0137 ($Aspm^{exon1\text{-}7}$) mice: (AA-F) 5′-GGGAAAGGCAAATGGAAAAC, (AA-Rgt) 5′-CCCAAGGCCATACAAGTGTT, and (AA-Rwt) 5′-ACCTCTCTGAGGAAGCACCA, with product size for WT allele 183 bp, gene trap allele 302 bp; for AJ0069 ($Aspm^{exon1\text{-}25}$) mice: (AJ-F) 5′-GAGACATAGCGGGTGAGAGC, (AJ-Rgt) 5′-CCTGGCCTCCAGACAAGTAG, and (AJ-Rwt) 5′-GCCTCACTAGCTGACACCACA, with product size for WT allele 161 bp, gene trap allele 307 bp.

Human *ASPM* transgenic mice were generated by pronuclear injection of a BAC that was linearized by NotI and purified on a Sepharose column. The BAC used (accession no. CTD-2353G2, vector pBELOBAC11) contains 136,600 bp of human genomic sequence, ≈41 kb of sequence 5′ to *ASPM* (downstream of the gene, because it is on the reverse strand), and 33 kb of sequence 3′ (upstream of the gene). Founder line screening and genotyping were performed by three primer pairs spanning the BAC: (L-F) 5′-ACACCCCACTGTCAATACTAGA, (L-R) 5′-GTCTTTGTCCTTACTGGGTTC, product size 404 bp; (M-F) 5′-CACCAGTGCTTGTAGGATAACT, (M-R) 5′-AGGAATCTAAGGTGTGCTAGTG, product size 601 bp; and (R-L) 5′-CACCTGAAGTTGGACCTTAAC, (R-R) 5′-TTGACCTACCTGACTGTAAACC, product size 767 bp.

Tis21-GFP knock-in mice were genotyped according to previously published protocols (5), and in experiments involving *Tis21*-GFP mice, a heterozygous background was used.

The day of the vaginal plug was defined as E0.5, and the day of birth was defined as postnatal day (P) 0.5.

RT-PCR. RT-PCR was performed using the OneStep RT-PCR Kit (Qiagen) on embryonic RNA extracted by the RNeasy Mini Kit (Qiagen). By using one forward primer targeting an exon upstream of the vector insertion site, and two reverse primers, one targeting the exon downstream of the insertion site and one targeting the 5′ end of β-geo, the endogenous transcript and the gene-trapped transcript could be distinguished. Primers for $Aspm^{exon1\text{-}7}$ mice: (exon6-F) 5′-CCGTACAGCTTGCTCCTTGT, (exon8-R) 5′-TCACTGTTGTCTGCCAGAGG, (5′_β-geo-R) 5′-GTTTTCCCAGTCACGACGTT with product size for WT transcript 231 bp, gene trap transcript 325 bp; for $Aspm^{exon1\text{-}25}$ mice: (exon25-F) 5′-TTTGTTGTGATCCGAAGCTG, (exon26-R) 5′-TCTCCAGGCTTCTCTCGGTA, (5′_β-geo-R) as above, with product size for WT transcript 179 bp, gene trap transcript 222 bp. Primers for mouse *Aspm*-specific RT-PCR: (Mm-F) 5′-AGCAGAAGCAGAATTCCTGTG, (Mm-R) 5′-TCCTTTTTGTCCCACACTGA, 211 bp; for human *ASPM*-specific RT-PCR: (Hs-F) 5′-GGTCCAAAGTTGTTGACCGTA, (Hs-R) 5′-CTTGCAGGGGATTTGTGATT; 219 bp.

Histology and Immunofluorescence Staining. Tissue dissection, fixation, cryosectioning, vibratome sectioning, immunofluorescence, and Nissl staining were performed as previously described (11). The following primary antibodies were used: Aspm (1), β-galactosidase (Z3781; Promega), Brn1 (sc-6028; Santa Cruz Biotechnology) (12), FoxP2 (ab16046; Abcam) (13), γ-tubulin (T6557; Sigma), Aurora B (611082; Becton Dickinson), phospho-histone H3 [06-570 (Millipore), ab10543 (Abcam)], phospho-vimentin (D076-3; MBL), pan-cadherin (C1821; Sigma), TuJ1 (mouse MMS-435P; rabbit MRB-435P; Covance), Tbr2 (ab23345; Abcam) (8), acetylated-α-tubulin (T6793; Sigma), MVH (ab13840; Abcam), and Nobox (ab41521; Abcam).

Quantification. Quantification of DAPI, PH3, pVim, *Tis21*-GFP, and Tbr2 staining was performed on 200-μm-wide fields of the dorsal telencephalon, with the ventricular surface being horizontal. For quantification of germ cells, P0.5 testes and adult ovaries were serially sectioned in a random orientation, and five sections spanning the organs were randomly chosen. MVH staining was used to identify gonocytes in testes, and Nobox staining to identify oocytes in ovaries.

Brain Size Measurements. Brains were dissected and weighed before fixation. For P0.5 mice, males and females were used, and for adult mice, to exclude heterogeneity caused by brain and body weight differences between male and female adult mice (www.jax.org/phenome), only males were used. For histological brain size measurements, brains were serially sectioned by a vibratome in the coronal orientation at 50-μm thickness. Nissl staining was performed on every fourth section in the region of interest (i.e., the cerebral cortex), such that a total of 15 sections were obtained for analysis. The area of the whole brain section and the area of the six-layered neocortex were measured using a Zeiss Axio Observer microscope and AxioVision software.

Electron Microscopy. Epididymides were dissected from 13-wk-old male mice and fixed in 1% glutaraldehyde and 2% paraformaldehyde in 0.1 M phosphate buffer at pH 7.4. The tissue was cut into small pieces, which were postfixed in 1% osmium tetroxide for 1 h at room temperature. Samples were dehydrated through a graded series of ethanol for standard embedding in EMBed-812 (Science Services). Ultrathin (70 nm) sections perpendicular to the epididymal tubules were cut on a Leica UCT ultramicrotome (Leica Microsystems), poststained with uranyl acetate and lead citrate, and viewed in a Morgagni electron microscope (FEI). Images were taken with a Veleta camera (Olympus).

In Situ Hybridization. In situ hybridization for mouse *Aspm* and human *ASPM* was performed using digoxigenin-labeled cRNA antisense probes, with human *ASPM* sense probe as a negative control, on cryosections by standard methods. Human *ASPM* probe corresponded to nucleotides 600–1,178 of the ORF, and mouse Aspm probe as previously described (1).

Protein Alignment and Domain Identification. The C-terminal region of human ASPM (amino acids 3,235–3,477) adjacent to the last isoleucine-glutamine (IQ) repeat was subjected to a PSI-BLAST search (14) using standard settings. The sequence picked up Armadillo repeats already at the second iteration. Multiple sequence alignments were done using ClustalW, and the alignment was manually refined and prepared for publication in Adobe Illustrator. Sequence accession nos. were as follows: *Homo sapiens* (NP_060606); *Pan troglodytes* (NP_001008994); *Macaca mulatta* (NP_001098005); *Equus caballus* (XP_001492636); *Bos taurus* (XP_614763); *Rattus norvegicus* (NP_001099425); and *Mus musculus* (NP_033921).

Fertility Testing. To analyze fertility, *Aspm* mutant males and females were paired with C57BL/6 females and males, respectively. Female mice in breeding cages were monitored daily for the presence of a vaginal plug, and when present were separated from the male. Pregnancy was assessed and embryo numbers were counted at postcoitum days 13.5 or 14.5 by dissection. The pregnancy rate was defined as the percentage of copulations resulting in pregnancy. WT mice, which were littermates to the mutant mice, were used as control. Some males were mated more than once. In some cases the mutant females were not dissected if nonpregnancy was obvious, were monitored that no pups were born, and then mated again to assess fertility. The mutant mice analyzed were between 8 and 25 wk of age, and the C57BL/6 mice used were between 8 and 15 wk of age, at the time of mating.

Sperm Analyses. To standardize the analysis of sperm, adult (8–12 wk old) virgin males were allowed to copulate once with a female as confirmed by vaginal plug, and were subjected to analysis 5 d later. To isolate sperm, intact epididymides were dissected, the surrounding fat tissue was carefully removed in 0.9% (wt/vol) NaCl, both epididymides were transferred to 170 μL cryoprotecting agent (CPA) solution [composed of 18% raffinose (R0250; Sigma) and 3% skim milk (0032-17-3; Difco)], ruptured with forceps, and incubated for 5 min at room temperature to release sperm. An aliquot (2 μL) of this sperm-containing suspension was transferred to 198 μL of HTF solution (15) and incubated for 5 min at 37 °C. An aliquot (25 μL) was taken and applied to Leja Standard Count 2 Chamber 100 Micron slides, and measurements were made on the IVOS Sperm Analyzer (Hamilton Thorne, version 12.3), with default settings for mouse sperm. In the case of the two homozygous mutants, measurements were also made, in parallel, with a 10-times-lower dilution factor (20 μL sperm-containing suspension into 180 μL HTF), to ensure similar levels of sperm sampling as WT for the acquisition of sperm velocity and morphology parameter data.

Statistics. Data processing, statistical analysis, and graph plotting were performed using the statistical programming language R (www.r-project.org). Student's *t* test was used for the calculation of all *P* values, with the exception of data with categorical variables: proportion of symmetric and asymmetric cell division (Fig. S4*E*), and the pregnancy rate data (Fig. 2 in main text), for which Fisher's exact test was used.

1. Fish JL, Kosodo Y, Enard W, Pääbo S, Huttner WB (2006) Aspm specifically maintains symmetric proliferative divisions of neuroepithelial cells. *Proc Natl Acad Sci USA* 103: 10438–10443.
2. Kouprina N, et al. (2005) The microcephaly ASPM gene is expressed in proliferating tissues and encodes for a mitotic spindle protein. *Hum Mol Genet* 14:2155–2165.
3. Paramasivam M, Chang YJ, LoTurco JJ (2007) ASPM and citron kinase co-localize to the midbody ring during cytokinesis. *Cell Cycle* 6:1605–1612.
4. Kosodo Y, et al. (2004) Asymmetric distribution of the apical plasma membrane during neurogenic divisions of mammalian neuroepithelial cells. *EMBO J* 23:2314–2324.
5. Haubensak W, Attardo A, Denk W, Huttner WB (2004) Neurons arise in the basal neuroepithelium of the early mammalian telencephalon: A major site of neurogenesis. *Proc Natl Acad Sci USA* 101:3196–3201.
6. Noctor SC, Martínez-Cerdeño V, Ivic L, Kriegstein AR (2004) Cortical neurons arise in symmetric and asymmetric division zones and migrate through specific phases. *Nat Neurosci* 7:136–144.
7. Miyata T, et al. (2004) Asymmetric production of surface-dividing and non-surface-dividing cortical progenitor cells. *Development* 131:3133–3145.
8. Englund C, et al. (2005) Pax6, Tbr2, and Tbr1 are expressed sequentially by radial glia, intermediate progenitor cells, and postmitotic neurons in developing neocortex. *J Neurosci* 25:247–251.
9. Hendzel MJ, et al. (1997) Mitosis-specific phosphorylation of histone H3 initiates primarily within pericentromeric heterochromatin during G2 and spreads in an ordered fashion coincident with mitotic chromosome condensation. *Chromosoma* 106:348–360.
10. Kamei Y, et al. (1998) Visualization of mitotic radial glial lineage cells in the developing rat brain by Cdc2 kinase-phosphorylated vimentin. *Glia* 23:191–199.
11. Pulvers JN, Huttner WB (2009) Brca1 is required for embryonic development of the mouse cerebral cortex to normal size by preventing apoptosis of early neural progenitors. *Development* 136:1859–1868.
12. McEvilly RJ, de Diaz MO, Schonemann MD, Hooshmand F, Rosenfeld MG (2002) Transcriptional regulation of cortical neuron migration by POU domain factors. *Science* 295:1528–1532.
13. Ferland RJ, Cherry TJ, Preware PO, Morrisey EE, Walsh CA (2003) Characterization of Foxp2 and Foxp1 mRNA and protein in the developing and mature brain. *J Comp Neurol* 460:266–279.
14. Altschul SF, et al. (1997) Gapped BLAST and PSI-BLAST: A new generation of protein database search programs. *Nucleic Acids Res* 25:3389–3402.
15. Quinn P, Kerin JF, Warnes GM (1985) Improved pregnancy rate in human in vitro fertilization with the use of a medium based on the composition of human tubal fluid. *Fertil Steril* 44:493–498.

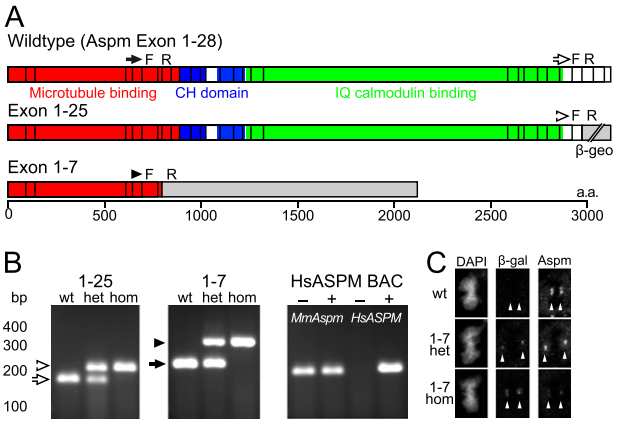

Fig. S1. *Aspm* mutant mice and *ASPM* humanized mice. (*A*) Scheme of mouse *Aspm* gene trap mutant proteins; WT, with 28 exons (*Top*), Aspm$^{exon1-25}$ (*Middle*), and Aspm$^{exon1-7}$ (*Bottom*). The major domains are indicated in colors, β-galactosidase/neomycin phosphotransferase (β-geo) in gray, and vertical lines separate exons. Arrows and arrowheads indicate primer pairs, the positions of which are indicated by letters (F, forward; R, reverse), and correspond to the RT-PCR products described in *B*. (*B*) RT-PCR on E13.5 whole-embryo RNA from *Aspm*$^{exon1-25}$ (*Left*), *Aspm*$^{exon1-7}$ (*Middle*), and human *ASPM* BAC transgenic (*Right*) mice. RT-PCR products are as follows: for *Aspm*$^{exon1-25}$, WT allele (179 bp) open arrow, gene-trapped allele (222 bp) open arrowhead; for *Aspm*$^{exon1-7}$, WT allele (231 bp) arrow, gene-trapped allele (325 bp) arrowhead; for human *ASPM* BAC transgenic (+) and littermate WT (–) mice, mouse *Aspm* (211 bp), human *ASPM* (219 bp). (*C*) Double immunofluorescence for β-gal and Aspm combined with DAPI staining of coronal cryosections (maximum intensity projection of three 1-μm optical sections) of E10.5 dorsal telencephalon. Note the colocalization of β-gal and Aspm immunoreactivity at the metaphase spindle poles (arrowheads) in the heterozygote and homozygote, demonstrating the tagging of the endogenous Aspm protein. Image width, 8.5 μm.

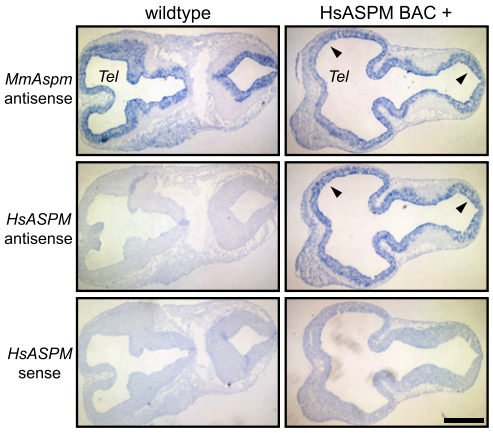

Fig. S2. *ASPM* BAC directs expression of human *ASPM* in transgenic mice with the same spatial pattern as endogenous mouse *Aspm*. In situ hybridization on transverse cryosections of E10.5 neural tube of WT (*Left*) and human *ASPM* BAC transgenic (HsASPM BAC +, *Right*) mice, from an independent founder line. Probes were as follows: mouse *Aspm*-specific antisense (*Top*), human *ASPM*-specific antisense (*Middle*), and human *ASPM*-specific sense (*Bottom*). Note the expression of human *ASPM* in the transgenic embryo, with the same spatial pattern as mouse *Aspm* (arrowheads). *Tel*, telencephalon. (Scale bar, 200 μm.)

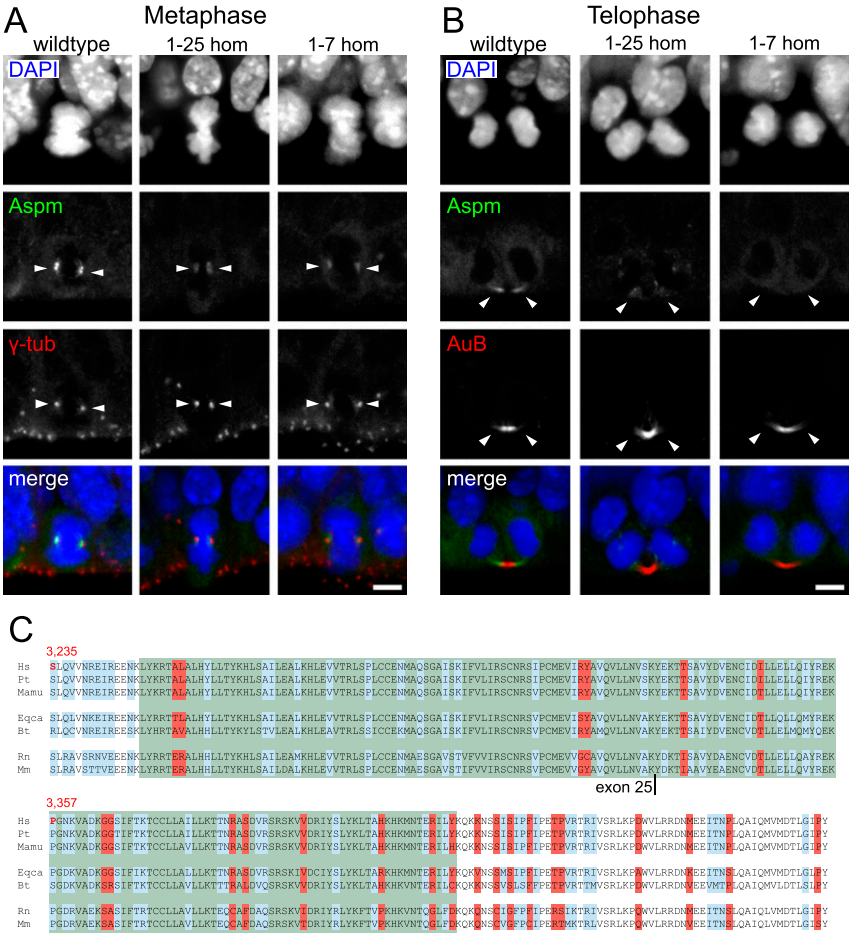

Fig. S3. Midbody localization defects caused by lack of Aspm C-terminal region. (*A* and *B*) Double immunofluorescence for Aspm (green) with γ-tubulin (γ-tub, red) in *A* and with Aurora B (AuB, red) in *B*, combined with DAPI staining (blue) of coronal cryosections (maximum intensity projection of two 1-μm optical sections) of E11.5 dorsal telencephalon of WT (*Left*) and *Aspm*$^{exon1-25}$ (*Middle*) and *Aspm*$^{exon1-7}$ (*Right*) homozygous mice. Cells in metaphase are shown in *A* and telophase in *B*. Note the Aspm immunoreactivity in the pericentrosomal region of cells in metaphase, indicated by arrowheads in *A*. Cells in telophase show Aspm immunoreactivity at the midbody, indicated by arrowheads in *B*, which is reduced in the *Aspm*$^{exon1-25}$ mutant and lacking in the *Aspm*$^{exon1-7}$ mutant. (Scale bar, 5 μm.) (*C*) Sequence alignment of mammalian Aspm proteins. Numbers refer to the amino acid residue in the human sequence (red letters). The region identifying Armadillo repeats is highlighted in green. Amino acids that differ between mammalian Aspm proteins are highlighted in blue and red. Blue indicates moderate and red indicates strong physico-chemical changes. Black line indicates the end of exon 25. Hs, human; Pt, chimpanzee; Mamu, macaque; Eqca, horse; Bt, cow; Rn, rat; Mm, mouse.

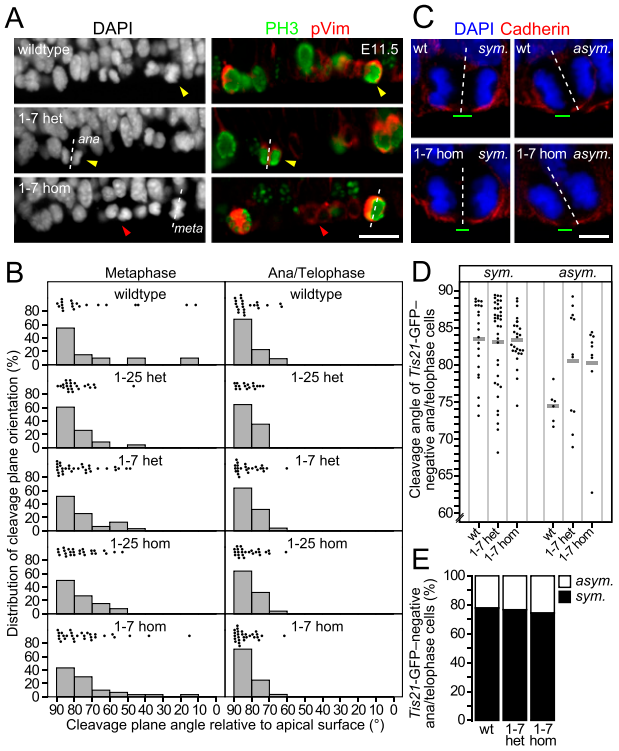

Fig. S4. Analysis of orientation and modes of neuroepithelial cell division in *Aspm* mutant mice. (*A*) Double immunofluorescence for phospho-histone H3 (PH3, green) and phospho-vimentin (pVim, red), combined with DAPI staining (white), of coronal cryosections (3-μm optical sections) of E11.5 dorsal telencephalon of WT and *Aspm*$^{exon1-7}$ heterozygous (het) and homozygous (hom) mice. Yellow arrowheads, double-positive cells; red arrowheads, pVim single-positive cell. Dashed lines indicate the predicted cleavage plane orientation quantified in *B*; meta, metaphase; ana, anaphase. (Scale bar, 20 μm.) (*B*) Histogram of the cleavage plane orientation, categorized into 10° bins (90°–81°, etc.) of apical mitotic cells in E11.5 dorsal telencephalon, as predicted by chromatid orientation in metaphase (*Left*) and anaphase or telophase (*Right*), defined by DAPI staining. Ninety degrees was defined as perpendicular to the ventricular surface. Single values (dots) are plotted above the histograms. For metaphase (from top), n = 20, 23, 31, 26, and 30 cells; ana/telophase (from top), n = 22, 17, 25, 25, and 28 cells; from four embryos per genotype. (*C*) Immunofluorescence for pan-cadherin (red) combined with DAPI staining (blue) of coronal cryosections (1-μm optical sections) of E11.5 dorsal telencephalon of WT and *Aspm*$^{exon1-7}$ homozygous (1-7 hom) mice in a *Tis21*-GFP heterozygous background (Fig. S5*A*). Dashed lines indicate the predicted cleavage plane; green bars indicate the cadherin hole. Symmetrically dividing (*sym.*, cadherin hole bisecting, *Left*) and asymmetrically dividing (*asym.*, cadherin hole bypassing, *Right*) cells are shown. (Scale bar, 5 μm.) (*D*) Quantification of the cleavage plane angle of symmetrically dividing (*sym.*) and asymmetrically dividing (*asym.*) *Tis21*-GFP–negative cells in anaphase or telophase determined as shown in *C*. Single data points (dots) are shown for WT, *Aspm*$^{exon1-7}$ (1-7) heterozygous (het) and homozygous (hom) mice. Horizontal bars indicate the mean. Data from: wt, 27; het; 47; hom; 35 cells, from three embryos per genotype. (*E*) Quantification of the proportion of symmetric (black columns) and asymmetric (white columns) cell divisions of *Tis21*-GFP–negative cells in anaphase or telophase, from WT, *Aspm*$^{exon1-7}$ (1-7) heterozygous (het) and homozygous (hom) mice. No significant changes were observed. Values were obtained from the data shown in *D*.

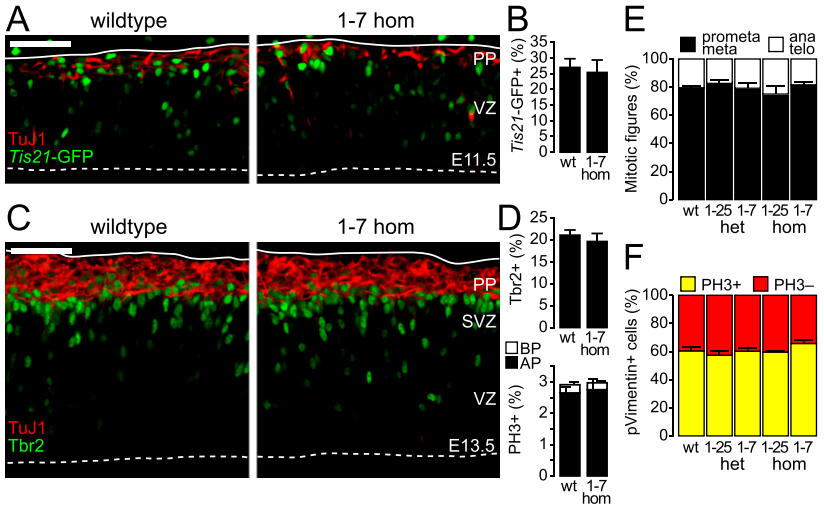

Fig. S5. Analysis of neural progenitor proliferation and differentiation in *Aspm* mutant mice. (*A*) Immunofluorescence staining for TuJ1 (red) with intrinsic *Tis21*-GFP fluorescence (green) of coronal cryosections (3-μm optical sections) of E11.5 dorsal telencephalon of WT (*Left*) and $Aspm^{exon1\text{-}7}$ homozygous (1-7 hom, *Right*) mice. VZ, ventricular zone; PP, preplate. (Scale bar, 50 μm.) (*B*) Quantification of *Tis21*-GFP–positive nuclei, expressed as a percentage of total nuclei as revealed by DAPI staining, in the VZ of E11.5 dorsal telencephalon of WT and $Aspm^{exon1\text{-}7}$ homozygous (1-7 hom) *Tis21*-GFP heterozygous mice. Data are the mean of three embryos (sum of three 200-μm-wide fields per embryo); error bars indicate SEM. (*C*) Double immunofluorescence staining for Tbr2 (green) and TuJ1 (red) of coronal cryosections (3-μm optical sections) of E13.5 dorsal telencephalon of WT (*Left*) and $Aspm^{exon1\text{-}7}$ homozygous (1-7 hom, *Right*) mice. SVZ, subventricular zone. (Scale bar, 50 μm.) (*D*) Quantification of Tbr2-positive nuclei, expressed as a percentage of total nuclei as revealed by DAPI staining, in the cortical wall of E13.5 dorsal telencephalon of WT and $Aspm^{exon1\text{-}7}$ homozygous (1-7 hom) mice (*Upper*), and quantification of PH3-positive apical (black column segments) and basal (white column segments) progenitor cells as a percentage of total nuclei in the VZ plus SVZ of E13.5 dorsal telencephalon of WT and $Aspm^{exon1\text{-}7}$ homozygous (1-7 hom) mice (*Lower*). Data are the mean of three embryos (sum of three 200-μm-wide fields per embryo); error bars indicate SEM. (*E*) Quantification of apical prometaphase plus metaphase cells (black column segments) and anaphase plus telophase cells (white column segments) expressed as a percentage of all apical mitotic cells, as determined by DAPI staining, in E11.5 dorsal telencephalon of WT and $Aspm^{exon1\text{-}25}$ (1-25) and $Aspm^{exon1\text{-}7}$ (1-7) heterozygous (het) and homozygous (hom) mice (Fig. S4*A*). Data are the mean of four embryos (sum of five 200-μm-wide fields per embryo); error bars indicate SEM. (*F*) Quantification of apical PH3 and pVim double-positive cells (yellow column segments) and apical pVim single-positive cells (red column segments), both expressed as a percentage of all apical pVim-positive cells, in E11.5 dorsal telencephalon of WT and $Aspm^{exon1\text{-}25}$ (1-25) and $Aspm^{exon1\text{-}7}$ (1-7) heterozygous (het) and homozygous (hom) mice (Fig. S4*A*). Data are the mean of four embryos (sum of five 200-μm-wide fields per embryo); error bars indicate SEM.